Coordinated Behavior of Mitochondria in Both Space and Time: A Reactive Oxygen Species-Activated Wave of Mitochondrial Depolarization

Nathan R. Brady,*†‡ Steven P. Elmore,† Johannes J. H. G. M. van Beek,† Klaas Krab,* Pierre J. Courtoy,§ Louis Hue,‡ and Hans V. Westerhoff*

*Department of Molecular Cell Physiology, The Centre for Research on BioComplex Systems, BioCentrum Amsterdam, NL-1081 HV, Amsterdam, The Netherlands; †Laboratory for Physiology, Institute for Cardiovascular Research, VU University Medical Center, NL-1081 BT, Amsterdam, The Netherlands; and ‡Hormone and Metabolic Research Unit and §Cell Biology Unit, Institute of Cellular Pathology and University of Louvain Medical School, B-1200 Brussels, Belgium

ABSTRACT Reactive oxygen species (ROS) can trigger a transient burst of mitochondrial ROS production via ROS activation of the mitochondrial permeability transition pore (MPTP), a phenomenon termed ROS-induced ROS release (RIRR). The goal of this study was to investigate if the generation of ROS in a discrete region of a cardiomyocyte could serve to propagate RIRR-mediated mitochondrial depolarizations throughout a cell. Our experiments revealed that localized RIRR activated either RIRR-mediated fluctuations in mitochondrial membrane potential (time period: 3–10 min) or a traveling wave of depolarization of the cell's mitochondria (velocity: ~5 μm/min). Both phenomena appeared to be mediated by the mitochondrial permeability transition pore and eventually encompassed the majority of the mitochondrial population of both isolated rat and rabbit cardiomyocytes. Furthermore, depolarization was often reversible; the waves of depolarization were then followed by a rapid (~40 μm/min) repolarization wave of the mitochondria. We show that the RIRR can function to communicate the mitochondrial permeability transition from one mitochondrion to another in the isolated adult cardiomyocyte.

INTRODUCTION

Reactive oxygen species (ROS) can trigger a transient increase in mitochondrial ROS production via ROS activation of the mitochondrial permeability transition pore (MPTP), a phenomenon termed ROS-induced ROS release (RIRR) (Zorov et al., 2000). Although definitive proof has not been established, it is widely considered that the MPTP is composed of the voltage dependent anion channel (VDAC), located in the outer mitochondrial membrane, the adenine nucleotide translocase (ANT), located in the inner mitochondrial membrane (IMM), and cyclophilin D, located in the mitochondrial matrix (see review by Crompton, 1999). Under conditions that lead to RIRR, an increase in ROS triggers the MPTP, possibly via the oxidation of thiol groups on the ANT, which in turn leads to the simultaneous collapse of mitochondrial membrane potential ($\Delta\Psi$) and an increased ROS generation by the electron transport chain (ETC) (Zorov et al., 2000). As such, RIRR constitutes a positive feedback mechanism for enhanced ROS production.

It has also been shown that under conditions of increased ROS production, superoxide anion is released from the mitochondrial matrix via inner membrane anion channels to the cytosol (Kulisz et al., 2002), and thus ROS could potentially function as a second messenger to activate RIRR in neighboring mitochondria. In fact, since the first reports of MPTP-mediated production of ROS, the presence of a mitochondrion-to-mitochondrion, RIRR-mediated signaling pathway has been hypothesized (Lemasters et al., 1998) and alluded to (Leach et al., 2001). However, direct evidence is lacking.

To examine these processes and their mechanisms in living cells, we employed several cell-permeable, phenomenon-specific fluorescent dyes. Tetramethylrhodamine methyl ester (TMRM), an electrophoretically accumulating, fluorescent dye, was used to assess the energetic state of mitochondria (Lemasters et al., 1998). Its photoexcitation was also used to generate sufficient levels of ROS to activate the MPTP (Huser et al., 1998; Huser and Blatter, 1999; Zorov et al., 2000; De Giorgi et al., 2002). To establish the participation of the MPTP, we employed calcein-AM, a fluorescent marker for MPTP activation (Nieminen et al., 1995), and cyclosporin A (CsA), a specific inhibitor of the MPTP (Lemasters et al., 1998). The presence of ROS was detected using 2′,7′-dichlorodihydrofluorescein diacetate ($DCFH_2$-DA) (Swift and Sarvazyan, 2000) and BODIPY $C11^{581/591}$ (Pap et al., 1999). As we wished to follow changes in mitochondrial bioenergetics in a cell where the mitochondria are located at fixed positions in well-defined arrays, the isolated adult cardiomyocyte was chosen as our experimental model (Duchen et al., 1998; Zorov et al., 2000).

In the study presented here, we investigated, in both isolated rat and rabbit cardiomyocytes, whether a localized, intracellular production of ROS could cause the propagation of ROS-induced depolarizations through an array of mitochondria in a living cell. Laser scanning confocal microscopy (LSCM) was used to locally generate ROS in the

Submitted September 22, 2003, and accepted for publication May 20, 2004.

Address reprint requests to Hans V. Westerhoff, Tel.: 31-20-4447230; Fax: 31-20-4447229; E-mail: hans.westerhoff@falw.vu.nl.

0006-3495/04/09/2022/13 $2.00

doi: 10.1529/biophysj.103.035097

mitochondria within a defined region of a cardiomyocyte and then to record the spatiotemporal responses of 1), $\Delta\Psi$, 2), ROS generation, and 3), the activation of the MPTP in the other mitochondria of the same confocal plane.

We demonstrate that local ROS production resulted in a cell-wide wave of concurrent mitochondrial depolarization, mitochondrial ROS production, and activation of the MPTP, as evidenced using specific fluorescent dyes. This wave was blocked by pretreatment with CsA, vitamin E, Trolox, 4,4′-diisothiocyanato-stilbene-2,2′-disulfonate (DIDS), and rotenone. These data present evidence that MPTP can serve to coordinate intracellular mitochondrial ROS production.

EXPERIMENTAL PROCEDURES

Preparation of cardiomyocytes

Rabbit cardiomyocytes were isolated from New Zealand white rabbit (3–6 month old) by collagenase digestion as previously described (Verheijck et al., 1999). Cells were suspended in HEPES-buffered solution (in mM: 137 NaCl, 4.9 KCl, 1.2 $MgSO_4$, 1.2 NaH_2PO_4, 1.8 $CaCl_2$, 15 glucose, 20 HEPES; pH 7.4) and stored at room temperature (RT) until use the same day.

Rat cardiomyocytes were isolated from Sprague Dawley rats (250–400 g) by collagenase digestion, as previously described (Lefebvre et al., 1996), and attached to laminin-coated coverslips (30 min incubation with 30 mg/l laminin and air-dried for 30 min). Cells were kept until use in an air/5% CO_2 incubator at 37°C in Medium 199 (M199) supplemented with 0.1 nM thyroxin, 0.10 μM insulin, 1.0 mM creatine, 1.0 mM taurine, 0.2% bovine serum albumin (BSA) and 10 units/ml penicillin, and 10 g/l streptomycin. All experiments were performed within 24 h of plating and at room temperature in HEPES-buffered solution (in mM: 120 NaCl, 4.7 KCl, 1.2 KH_2PO_4, 1.25 $MgSO_4$, 1.0 $CaCl_2$, 15 glucose, 20 Na-HEPES; pH 7.4).

Loading conditions

Rabbit cardiomyocytes were loaded with fluorescent dyes for 30 min in HEPES-buffered M199 (supplemented with 1% BSA) at 37°C. Due to equipment and time concerns, we developed a protocol allowing for immediate imaging utilizing agarose: cells were centrifuged momentarily to remove medium, mixed with 0.2% agarose (~37°C; M199 and 1% BSA), and then deposited onto glass-well plates (MatTek, Ashland, MD). Rat cardiomyocytes were loaded with the fluorescent dyes in M199 medium at 37°C, or HEPES-buffered solution at room temperature, and let to equilibrate for 30 min before imaging, with the exception of calcein-AM, which was incubated at 37°C for 15 min to ensure cytosolic loading. The medium was removed and replaced with the HEPES-buffered solution after incubation with the fluorescent dyes. Cells were incubated with DIDS, BAPTA-AM, vitamin E, Trolox, or CsA for at least 1 h before imaging. No differences were apparent, in response to a localized ROS production between agarose-plated, or laminin-plated, rabbit and laminin-plated rat cardiomyocytes.

Localized TMRM photoexcitation/ROS generation

Two approaches were used to generate ROS locally through laser excitation of TMRM: line scanning or use of the zoom function. As several confocal systems were used, each with differing laser powers and laser attenuation capabilities, we held as the criteria that scanning was applied until local depolarizations were observed. Line scanning was performed as described (Zorov et al., 2000). The zoom function was used to affect boxed regions, typically between 100 and 300 μm^2, and these regions were scanned 10–15 times at 1-s intervals. Laser power was held constant throughout both the ROS generation process and imaging period of the experiment, unless indicated otherwise.

Laser scanning confocal microscopy

Cardiomyocytes were selected according to the criteria that they be rod shaped and free of membrane blebs. Four laser scanning confocal microscopes were used: a Leica (Wetzlar, Germany) TCS-4D (krypton-argon laser), a Zeiss (Jena, Germany) 510 (helium-neon and argon lasers), a Bio-Rad (Hercules, CA) MRC1024 (argon laser), or a Bio-Rad Radiance 2000 (helium-neon and argon lasers). The confocal pinholes were configured to obtain images of 1 μm in the axial dimension.

Image analysis

When necessary, images were converted from the Bio-Rad PIC to AVI format using the public domain software ImageJ (http://rsb.info.nih.gov/ij) and Bio-Rad reader plugin. All single TIFF and AVI images and AVI stacks were imported into the Zeiss Image Browser R3.0 database (http://www.zeiss.de) and pseudocolored. Pinhole and image sizes were imported accordingly in order to calculate wave kinetics. The wave velocities were calculated by measuring wave progression, in the longitudinal direction, between time frames. Statistical analyses are represented as averages $\pm$ standard deviation. Under given conditions and as indicated, n refers to the number of cardiomyocytes or mitochondria imaged.

Materials

All dyes and reagents were purchased from Calbiochem (San Diego, CA) and Molecular Probes (Eugene, OR). DIDS, CsA, and Trolox were purchased from Calbiochem. Rotenone, media, and other reagents were purchased from Sigma (St. Louis, MO).

RESULTS

Cardiomyocytes serve as a model to study spatial and temporal dynamics of mitochondrial energetics

To demonstrate the mitochondrial spatial organization in cardiomyocytes, rat cells were incubated with the electrophoretically accumulating TMRM and imaged by LSCM. Fig. 1 demonstrates the manner in which mitochondria are organized longitudinally along the myofibrils and laterally between sarcomeric Z-lines, as previously shown by electron microscopy (e.g., Nozaki et al., 2001). Thus, in addition to being prone to RIRR (Zorov et al., 2000), the precise positioning of the isolated cardiomyocyte mitochondria makes them highly suitable for high-resolution spatial and temporal studies. From confocal images of TMRM-labeled cardiomyocytes (e.g., Fig. 1), we calculated that longitudinally the mitochondria had a length of ~1.2 μm and were separated by ~0.4-μm gaps (Table 1). Although such calculations can be influenced by the limited spatial resolution of the microscope, these live-cell imaging results are in close agreement with mitochondrial lengths and intermitochondrial gaps of cardiomyocytes, as determined on aldehyde-fixed tissue by electron microscopy (Nozaki et al., 2001).

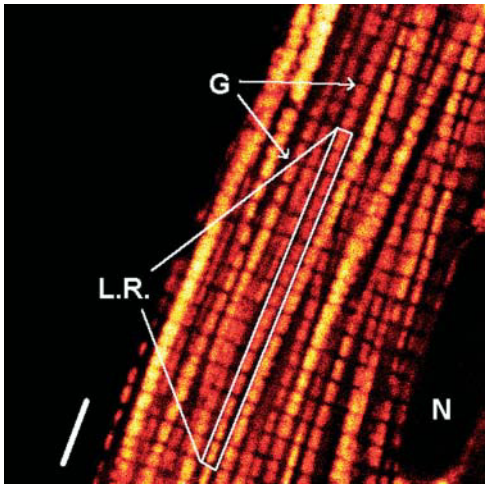

FIGURE 1 Organization of the mitochondria of an isolated cardiomyocyte. A rat cardiomyocyte was loaded with 0.2 μM TMRM, and a 0.7-μm optical section of the cell was imaged at a high spatial resolution (3× Kalman averaging). This figure is representative of images used to calculated characteristics of mitochondria arranged longitudinally along the myofibrils (Table 1). L.R. is an example of a measured longitudinal row, N is a nucleus, and G refers to the longitudinal gaps between mitochondria. Scale bar = 5 μm.

Localized confocal imaging as a tool to produce a local ROS insult

In addition to its use as an indicator of changes in the electric potential across the IMM, photoexcitation of TMRM results in production of singlet oxygen ($^1O_2$), superoxide anion ($\cdot O_2^-$), and hydroxyl radical (OH·) (Zorov et al., 2000). The probe $DCFH_2$-DA, which is oxidized to green fluorescing DCF by H_2O_2 or OH, was used as a marker for ROS generation (Swift and Sarvazyan, 2000). Note, although Swift and Sarvazyan demonstrated a possible FRET interaction between MitoTracker Red and DCF, we found that the addition of 0.1–0.2 μM TMRM did not have an appreciable effect on DCF fluorescence (10.0 μM preloaded 30 min at RT; N. R. Brady and H. V. Westerhoff, unpublished data). Furthermore, in cardiomyocytes loaded with both 0.1 μM TMRM and 10.0 μM DCF, inducing the collapse of $\Delta\Psi$ with the uncoupler carbonyl cyanide p-(trifluoro-methoxy)phenylhydrazone did not increase DCF fluorescence, as would occur due significant FRET interaction (cf. Supplementary Material). Thus increases in DCF fluorescence that we report here were due to the oxidation of $DCFH_2$ to DCF and not due to the loss of FRET between DCF and TMRM.

TABLE 1 Characteristics of cardiomyocyte mitochondria arranged longitudinally along the myofibril

Per longitudinal row	
Average number of mitochondria/μm	0.62 (±0.04)
Average length of a mitochondrion	1.2 (±0.1) μm
Average longitudinal distance between two mitochondria	0.4 μm
Average length of a cardiomyocyte	118 (±16) μm
Average number of mitochondria	73
Longitudinal space occupied by mitochondria	87 μm (74%)
Longitudinal space not occupied by mitochondria	30 μm (26%)

Data were calculated from five randomly selected images (e.g., Fig. 1).

To bring about a spatiotemporally controlled production of ROS, we excited a contiguous population of TMRM-loaded mitochondria (*boxed region* in Fig. 2 *A*). Imaging this region revealed that after a few seconds TMRM fluorescence began to diminish and an increase of the DCF fluorescence occurred over time. When inspecting single mitochondria, such as the one in Fig. 2 *B* (*circle*), we typically observed that during the first second or two $DCFH_2$ oxidation was minimal (Fig. 2 *C*, *s1*), and $\Delta\Psi$ remained intact. Then, TMRM photoexcitation triggered a sudden increase in the oxidation of $DCFH_2$ (Fig. 2 *C*, *shaded arrow intersection* of *s1* and *s2*) slightly before a sudden decrease in TMRM fluorescence (*solid arrow*). The collapse of $\Delta\Psi$ occurred over a time period of ~5 s for a rat mitochondrion and 4 s for a rabbit mitochondrion (Table 2) and correlated to a decrease in $DCFH_2$ oxidation (Fig. 2 *C*, *s3*). We interpret these drastic shifts in fluorescence as reflecting $\Delta\Psi$-dependent RIRR and ROS-induced membrane depolarization (cf. Zorov et al., 2000).

This response to intense TMRM photoexcitation was heterogeneous: not all mitochondria within the affected region underwent the sudden change in TMRM and DCF fluorescence simultaneously. Inspection of Fig. 2 *B* reveals red (*X*, polarized), yellow (*Y*, ROS producing), and green (*Z*, depolarized) mitochondria. This spatial heterogeneity demonstrates that the mitochondria of the isolated ventricular cardiomyocyte are not lumenally connected and exist as energetically independent units (see Supplementary Video 1).

The localized ROS insult triggered intracellular mitochondrial depolarizations, both in and adjacent to the initial depolarization

When $\Delta\Psi$ decreases, the changes in TMRM fluorescence can be equivocal. The exit of TMRM due to depolarization can either result in a decrease of fluorescence (Zorov et al., 2000) or in an increase of fluorescence when there is autoquenching (Boitier et al., 1999), depending on the degree of TMRM uptake into the mitochondria. Thus, in initial experiments, to observe changes in $\Delta\Psi$ we applied the technique of FRET from MitoTracker Green (MTG), which binds covalently to mitochondrial matrix sulfhydryl groups (Sutovsky et al., 1996), to TMRM. In the polarized mitochondrion, when solely exciting MTG with blue light, the FRET interaction between MTG and TMRM results in the quenching of MTG (green) fluorescence and excitation of TMRM (red). The efflux of TMRM from the matrix (depolarization) leads to reversal of the FRET interaction, resulting in both the loss of TMRM fluorescence and the unquenching (gain) of green, MTG fluorescence. Conversely, a green-to-red transition indicates repolarization (Elmore et al., 2001). Employing this FRET technique permitted a less

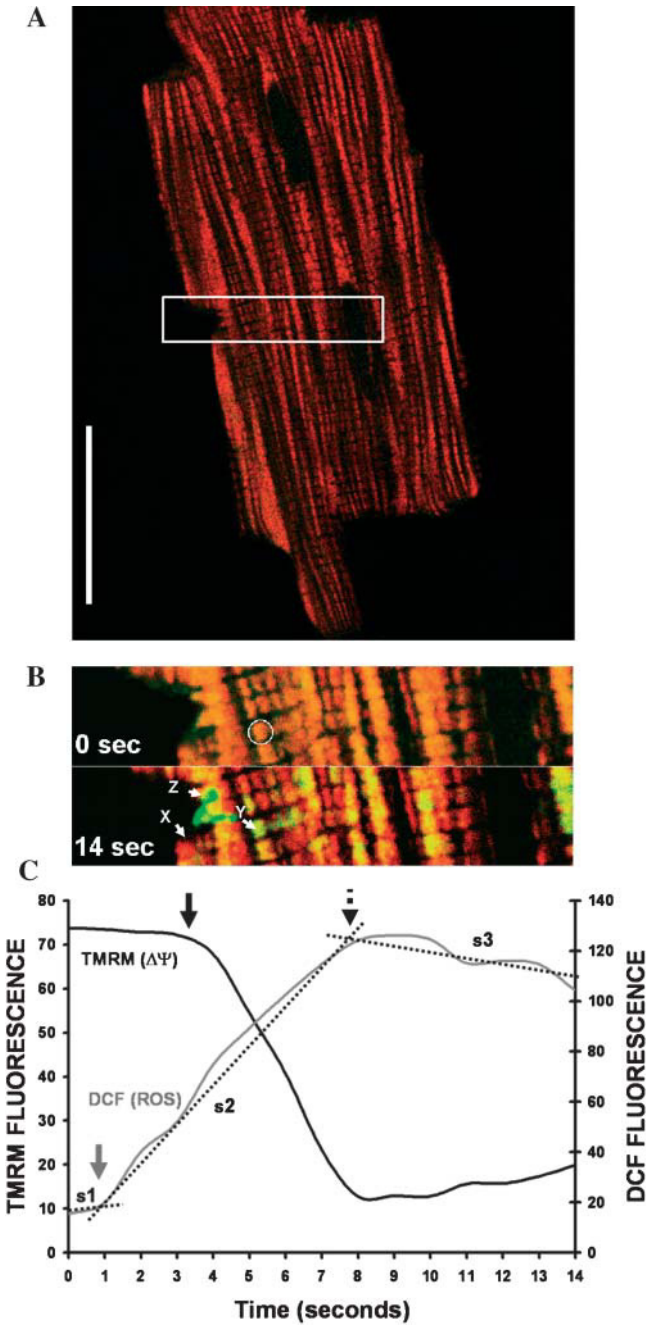

FIGURE 2 Localized photoexcitation of TMRM: dynamics of $\Delta\Psi$- and ROS production at the level of a single mitochondrion. The 0.2-μM TMRM and 10.0-μM DCF fluorescence were measured in mitochondria of a typical rat cardiomyocyte (as shown labeled with TMRM in *A*). (*B*) From $t = 0$ onwards, confocal imaging of DCF and TMRM fluorescence was confined to the region bounded by the white box and repeated each second, simultaneously recording the decrease in TMRM fluorescence (which reports changes in $\Delta\Psi$) and increase in DCF fluorescence (which reports on the presence of ROS). (*C*) The kinetics of depolarization and ROS production in a single mitochondrion (○ in *B*). The arrows (*shaded* for DCF and *solid* for TMRM) indicate the time points where a significant change occurred. Three lines (*s1*, *s2*, and *s3*) refer to the slopes (rates) of changes in DCF fluorescence. Arrow 1 (*shaded*) indicates the shift to a faster increase in DCF fluorescence (*intersection* of *s1* and *s2*), arrow 2 (*solid*) indicates the point at which $\Delta\Psi$ began to decrease, arrow 3 refers the point at which DCF fluorescence increase slowed and $\Delta\Psi$ had collapsed (*intersection* of *s2* and *s3*). See online Supplementary Material for an example movie. This is one experiment that is representative of more than three.

TABLE 2 Kinetics of mitochondrial depolarization and ROS production in response to a localized ROS production

Rabbit	
Our measured values, calculated from line scans	
Duration for MPTP-mediated depolarization	4 ± 2 s ($n = 5$ cells)
Duration of ROS bursting	7 ± 2 s ($n = 5$ cells)
Rat	
As determined previously by Zorov et al., 2000	
Duration for MPTP-mediated depolarization	~5 s
Duration of ROS bursting	5–10 s
Our measured values, calculated from sequential images (e.g., Fig. 2 *A*)	
Duration for MPTP-mediated depolarization	5 ± 2 s ($n = 7$ mitochondria and 4 cells)
Duration of ROS bursting	7 ± 3 s ($n = 5$ mitochondria and 3 cells)
Duration of an average wave = (average length of a cardiomyocyte (118 μm))/(calculated wave velocity of 5.4 μm/min)	21.9 min
Duration of wave in mitochondria = (average number of mitochondria per cell aligned longitudinally (73)) × (average ROS burst of 7 s)	8.5 min (39%)
Duration of wave in cytosolic space between mitochondria = (duration of average wave (21.9 min)) − (duration of mitochondrial wave (8.5 min))	13.4 min (61%)
Travel duration across the 0.4-μm cytosolic gap between mitochondria = (duration of cytosolic wave (13.4 min))/(no. of cytosolic gaps (73))	11 s

ambiguous method to initially assess changes in mitochondrial energetics in the cardiomyocyte than employing TMRM alone.

Before the localized production of ROS, excitation of MTG resulted primarily in red TMRM fluorescence through FRET, as also indicated by lack of green fluorescence (Fig. 3 *i*). After a brief, intense excitation of TMRM (543 nm) at one end of the cell (Fig. 3 *i*, *white boxed region*), red TMRM fluorescence decreased, and green MTG fluorescence increased in regions neighboring the mitochondria within the white box, evidencing mitochondrial depolarization. During a period of ~3 min (Fig. 3, *ii–vi*) the mitochondrial population underwent $\Delta\Psi$-fluctuations, as indicated by changes in red and green fluorescence, before returning to a sustained polarized state (increase in red and decrease in green).

Spatiotemporally correlated depolarization of the mitochondrial population, concomitant with the onset of the mitochondrial permeability transition

The MPTP is permeable to molecules up to 1.5 kDa (see review by Crompton, 1999). To establish if the MPTP

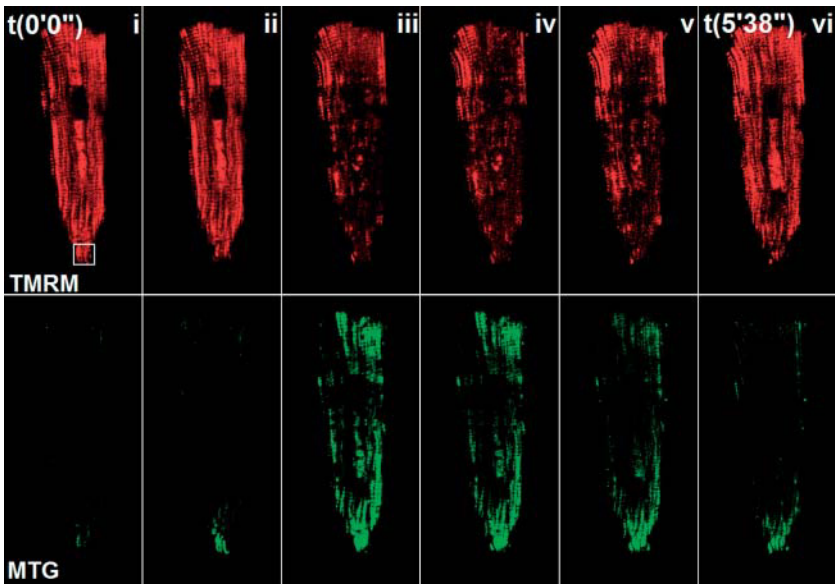

FIGURE 3 ROS-induced changes in mitochondrial membrane potential. Rabbit cardiomyocytes were dual loaded with 0.3 μM MTG and 0.7 μM TMRM. The FRET interaction between the MTG, covalently bound in the mitochondrial matrix, and the electrophoretically accumulating TMRM was used to image the energetic state of the mitochondria, via excitation of MTG at 488 nm and simultaneous recording of red and green fluorescence. Red fluorescence indicated a FRET interaction between MTG and TMRM, i.e., polarized mitochondria. The gain (unquenching) of green fluorescence indicated loss of TMRM from the mitochondria, i.e., mitochondrial depolarization. The requenching of green fluorescence was indicative of mitochondrial repolarization. ROS production was restricted to the area bounded by the white box (*i*) by intense laser scanning of TMRM at 568 nm, until TMRM fluorescence in the region began to decrease. As demonstrated by increased green fluorescence, intense photoexcitation activated mitochondrial depolarizations outside the area of primary ROS production (*i*). Nearly the entire mitochondrial population exhibited variations in $\Delta\Psi$ for ~5 min (*ii–v*), before returning to a polarized state (*vi*). Images were obtained with a Zeiss 510 LSCM. This is one experiment that is representative of three. Scale bar = 20 μm.

participated in ROS-activated mitochondrial depolarizations, we employed the fluorescent molecule calcein (620 Da). Calcein-AM was loaded into the isolated cardiomyocytes so as to accumulate preferentially in their cytosol (15 min, at 37°C). Under these conditions cytosolic endogenous esterases cleave the ester group of calcein-AM, thereby impeding its movement into the mitochondria or out of the cell. Activation of the MPTP should then result in the entry of calcein into the mitochondria (Nieminen et al., 1995).

When loaded cytosolically, the green-fluorescing calcein was apparent in the nuclei, there colocalizing with the red-fluorescing, cell-permeant nuclear stain Syto 83. In the cytosol there was green fluorescence in some parts but also a lack of green fluorescence in longitudinal rows (*LR*) and in the perinuclear regions (*P*). This distribution of calcein was due to the loading temperature, as calcein loaded at room temperature exhibited a homogeneous distribution (Fig. 4 *A*). In rabbit cardiomyocytes dual loaded with TMRM and calcein-AM, the TMRM-labeled mitochondria were located in these distinct voids in the green, fluorescently labeled cytosol (Fig. 4 *C*).

As the voids were also seen in cells loaded with calcein, but without TMRM (Fig. 4 *A*), the observed pattern of cytosolic loading of calcein was not an artifact caused by FRET between calcein and TMRM. When we subjected the cell to the usual protocol for localized ROS production (line scanning or zooming in), green calcein fluorescence increased in the mitochondria, simultaneous with loss of red TMRM fluorescence, thereby demonstrating a permeabilization of the IMM to calcein concomitant with depolarization (our unpublished data). After localized ROS production, the region around the original scanning line depolarized, as evidenced by loss of TMRM fluorescence. Spatially concurrent with the loss of TMRM fluorescence, calcein fluorescence spread homogeneously throughout the cell, entering what previously were voids. This evidenced the permeabilization of the IMM, consistent with the opening of the MPTP. In these cells, the calcein and TMRM fluorescent responses proceeded in a wave-like manner and ultimately involved the majority of the mitochondria of the cardiomyocyte (Fig. 4 *B*, *right panels*). The behavior of rat cardiomyocytes was comparable. The persistent black strip in Fig. 4 *B*, *right panels* we attribute to photobleaching of the calcein by the initial line scan. Together, we take these results to demonstrate that at the wave front the MPTP is activated, permeabilizing mitochondria to calcein.

In both rat and rabbit cardiomyocytes, we observed that in a few cases a progressive decrease in TMRM fluorescence evidenced the wave of depolarization, as usual, but then several minutes after the localized ROS insult, the previously depolarized region as well as the wave front showed an increase in TMRM fluorescence. This was not observed when the loading concentration of TMRM was decreased to 0.1 μM. Possibly then, in these cases depolarization and TMRM efflux reduced autoquenching. Importantly though, the wave of change in mitochondrial permeability was also seen in these cases: calcein entry into the neighboring mitochondria coincided with the wave and continued at the same velocity until the majority of the mitochondrial population in the cell had depolarized.

To further examine whether the MPTP was involved in the spread of depolarization from the region of laser-induced ROS production, cardiomyocytes were preincubated with CsA, an inhibitor of the MPTP (Lemasters et al., 1998).

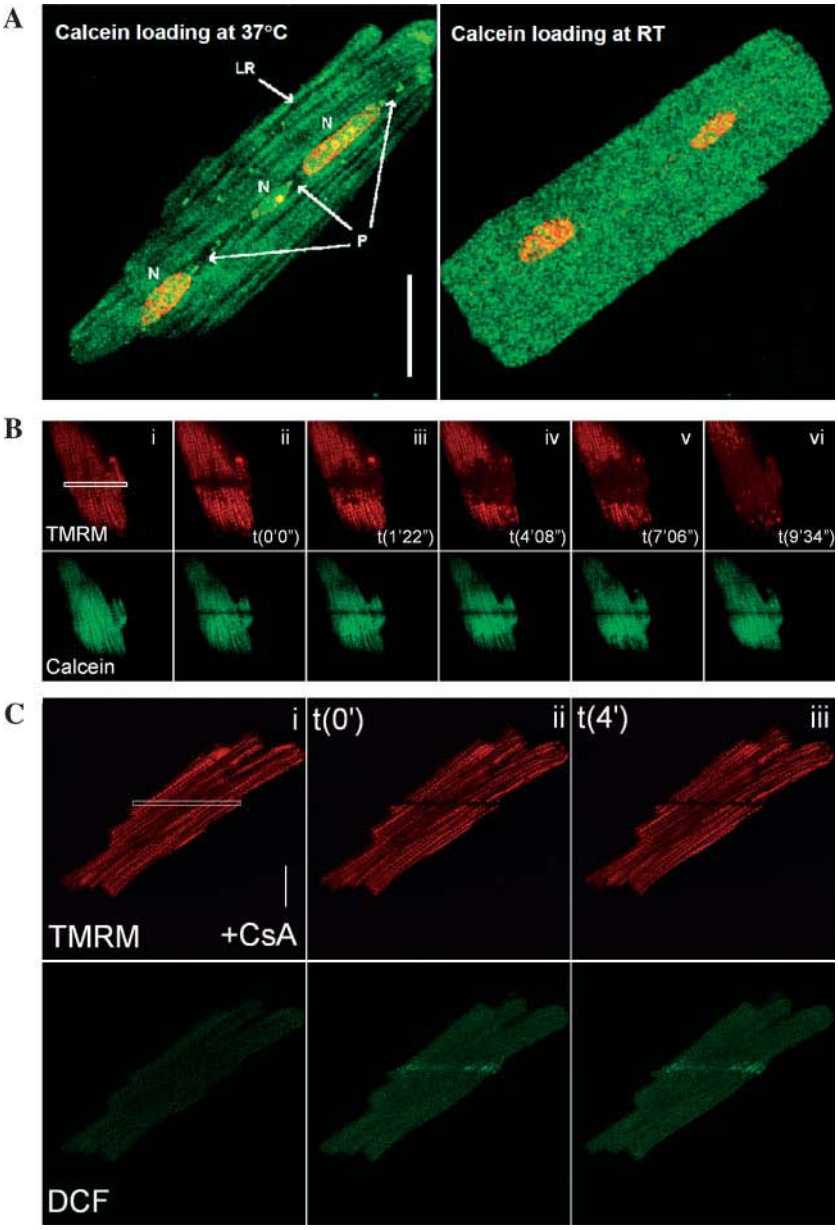

FIGURE 4 The cellular effect of a localized production of ROS: fluctuations and waves of mitochondrial depolarizations, concomitant with the activation of the MPTP. (*A*) Cardiomyocytes were incubated with 1.0 μM calcein-AM for (*left*) 15 min at 37°C or (*right*) 30 min at room temperature (*RT*). Calcein-containing medium was then removed and replaced with fresh medium containing 10 μM Syto 83, and cells were imaged 30 min later. In the warm-loaded cells, calcein fluorescence was observed in the nuclei (*N*), colocalizing with the red fluorescing nuclear stain Syto 83. However, calcein fluorescence was not observed in the perinuclear region (*P*) or in voids that run longitudinal rows (*LR*). In the RT-loaded cells, green fluorescing calcein was observed homogeneously throughout the cell. Images were obtained with a Bio-Rad Radiance 2000 LSCM. Scale bar = 20 μm. (*B, left panel*) Cardiomyocytes were dual loaded 15 min at 37°C with 0.20 μM TMRM and 1.0 μM calcein-AM, thereby resulting in the cytosolic distribution of calcein initially to be in excess over that in mitochondria. Before localized ROS production, calcein was more concentrated in the cytosol, and the mitochondria appear as voids in green, and red regions identify polarized mitochondria, as demonstrated by merging the TMRM and calcein images. (*B, right panels*) After the ROS production via line scanning, we observed localized loss of both TMRM (depolarization) and calcein fluorescence (photobleaching). Subsequently, the mitochondria depolarized as a function of distance from the region line scanned and green fluorescence appeared in regions previously labeled by TMRM (i.e., the mitochondria) demonstrating the participation of the MPTP (*ii–vi*). The wave of depolarization proceeded at ~5 μm/min. Images were obtained with a Leica TCS-4D LSCM. This is one experiment that is representative of more than three. Scale bars =20

Although CsA treatment did not prevent laser-induced localized ROS production (Fig. 4 *C*, *ii*), the spreading of depolarization into neighboring mitochondria was blocked at least for several minutes (Fig. 4 *C*, *iii*). CsA successfully inhibited the wave of depolarization in both rat and rabbit cardiomyocytes (rat: 1 μM, $n = 5$; rabbit: 3 μM, $n = 5$).

Spatiotemporal coincidence of mitochondrial depolarization and increased generation of reactive oxygen species

As ROS are known activators of the MPTP (see review by Zoratti and Szabo, 1995), we examined the spatiotemporal correlation between ROS production and mitochondrial depolarization. After the intense localized ROS production by TMRM photoexcitation (*boxed region* in Fig. 5 *A*, *i*), all mitochondria that had depolarized as shown by decreased TMRM fluorescence (*red*), also showed increased DCF fluorescence (*green*) (Fig. 5 *A*, *ii*), indicating an increased presence of ROS. Furthermore, the advance of the wave of depolarization correlated with a wave of increased DCF fluorescence, indicative of elevated ROS generation (Fig. 5 *A*, *iii–xvi*). Examination of a longitudinal row of mitochondria (*line* in Fig. 5 *A*, *i*) revealed that wave velocity was not constant, and, furthermore, mitochondria occasionally depolarized either before or after passage of the wave front (*arrows* in Fig. 5 *B*).

To support the findings employing $DCFH_2$, we used an additional fluorescent marker for ROS, BODIPY

$C11^{(581/591)}$. This probe contains a lipophilic moiety that causes it to incorporate into membranes. When oxidized, the molecule undergoes a fluorescence shift from red to green (Pap et al., 1999). As with DCF, an increase in green BODIPY $C11^{(581/591)}$ fluorescence in parallel to a decrease in red TMRM fluorescence confirmed that mitochondrial depolarization coincided with an increase in ROS production (Fig. 6, *ii–vi*). Remarkably, after the loss of fluorescence of nearly all mitochondria (Fig. 6 *vi*), there appeared to occur a redistribution and intensification of TMRM fluorescence (Fig. 6, *vii–viii*), which could signify mitochondrial repolarization. Such redistributions of TMRM were observed in several ($n = 8$ of 17) rabbit cardiomyocytes and occurred at a velocity of 45 ± 12 μm/min (calculated from three cells).

Additional evidence for a role of ROS was obtained using antioxidants and the ETC complex I inhibitor, rotenone. Preincubation of rat cardiomyocytes with 0.2 mM water-soluble vitamin E derivative Trolox, blocked the laser-induced ROS production and mitochondrial depolarization. Whereas preincubation of rabbit cardiomyocytes with 2 mM vitamin E did not block localized depolarization, it did halt the subsequent spread of the wave of depolarization (our unpublished data). Preincubation (30 min) with 1 μM rotenone required higher laser intensity and increased scanning time for the mitochondria within the initial region of interest to depolarize (our unpublished data). It also inhibited the progression of the wave of depolarization (Fig. 7).

Propagation of the mitochondrial depolarization either fluctuated or was wave-like

As shown above, after photoexcitation of TMRM within a defined region of a cardiomyocyte, local fluorescence decreased. Subsequently, we observed that a wave of depolarization emanated from the region that had been depolarized in the manner illustrated in Figs. 4–6. The wave of depolarization was found both in rat cardiomyocytes (observed in 13/23 cells subjected to the same laser excitation during the initial ROS production phase; velocity of 5.4 ± 1.5 μm/min, determined from seven cells) and in rabbit cardiomyocytes (14/17 cells; velocity of 5.2 ± 4.3 μm/min, determined from 10 cells). Velocities were calculated from a subset of cells where enough time points were correlated.

In rat cardiomyocytes, 10/23 tested cells showed a less organized spread of mitochondrial depolarization. Depolarization of either clusters of mitochondria or of individual mitochondria occurred at moments that did not always correlate with their distance from the site of initial laser-induced depolarization. These $\Delta\Psi$-fluctuations were observed to occur over a prolonged time (rat: 10.8 ± 3.4 min;

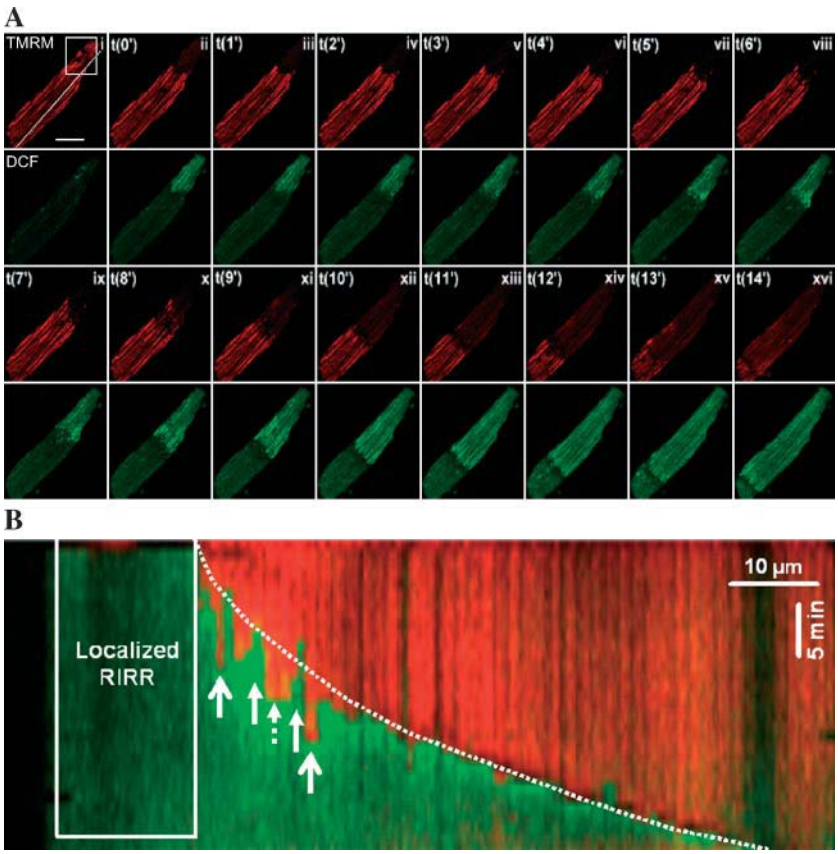

FIGURE 5 Depolarization coincided with increased production of ROS. (*A*) Rat cardiomyocytes were dual loaded with 10.0 μM $DCFH_2$-DA and 0.1 μM TMRM, and imaged every 30 s after a localized production of ROS (*box* in *i*). Basal ROS presence was low, as detected by the cell-permeant, green-fluorescent dye, $DCFH_2$-DA, which becomes fluorescent when oxidized to DCF (Swift and Sarvazyan, 2000) (*green*). ROS production sufficient to activate the MPTP was localized to the region bordered by the white box (*i*). Subsequently, a wave of mitochondrial depolarization occurred (*ii–x*) at an average velocity of ~5 μm/min. The mitochondrial depolarizations coincided with increased $DCFH_2$ oxidation; i.e., increased ROS production. See online Supplementary Material for full-length movie. (*B*) To observe the kinetics of wave progression through the cardiomyocyte changes in TMRM (*red*) and DCF (*green*) fluorescence were measured along a longitudinal row of mitochondria (*line* in *A*, *i*) through all time points imaged. Time is represented on the *y* axis, and the *x* axis corresponds to the row of mitochondria. The originally targeted region is represented by the box localized RIRR, and the wave progresses from left to right. Wave velocity is denoted by the dotted white line. Closed arrows indicate examples of mitochondria that remained polarized after passage of the wave front, and open arrows indicate examples of mitochondria depolarizing before passage of the wave front. Images were obtained with a Bio-Rad Radiance 2000 LSCM. This is one experiment that is representative of more than three. Scale bar = 20 μm.

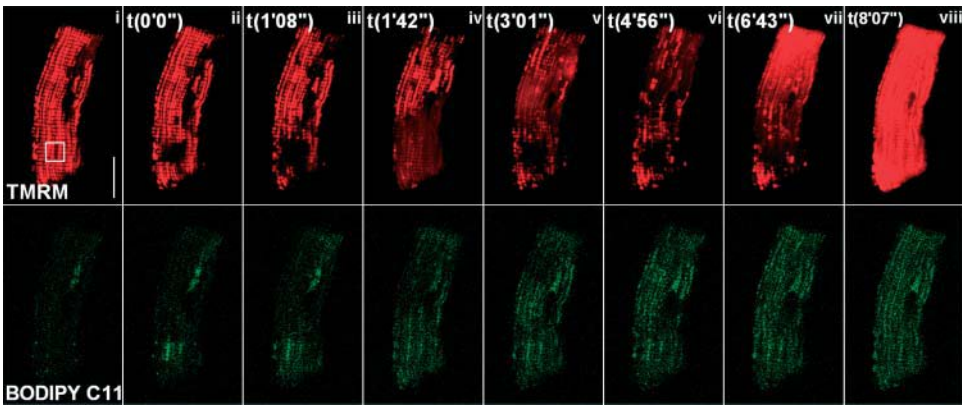

FIGURE 6 Depolarization coincided with increased lipid peroxidation. Rabbit cardiomyocytes were dual loaded with 0.5 μM BODIPY C11$^{(581/591)}$ and 0.2 μM TMRM. The presence of ROS was detected with the lipophilic, red fluorescent dye, BODIPY C11$^{(581/591)}$. This probe embeds into membranes and upon oxidation undergoes red-to-green shift and can therefore be used as a marker for lipid peroxidation (Pap et al., 1999). The cell was scanned (543 nm) in the region bordered by the white box (*i*) until mitochondria locally depolarized. After localized production of ROS due to photoexcitation of TMRM, a wave of depolarization proceeded at a velocity of ~5 μm/min (*ii–vi*). The mitochondrial depolarizations (indicated by loss of red fluorescence) coincided with increased green BODIPY C11$^{(581/591)}$ fluorescence; i.e., increased lipid peroxidation (*ii–vi*). After the wave of depolarization, the mitochondrial population repolarized at a velocity of ~40 μm/min (*vii–viii*). Images were obtained with a Zeiss 510 LSCM. This is one experiment that is representative of three. Scale bar = 20 μm.

$n = 10$; rabbit: 3 min; $n = 3$) and involved most mitochondria. To understand this differential response to a localized ROS production, of waves versus fluctuations, we varied the ROS insult by changing the initial laser excitation but kept the laser intensity during the imaging periods the same. In rat cardiomyocytes, increasing laser power by 10-fold, during the localized ROS production phase, augmented the incidence of a coherent wave of depolarization (to $n = 6/7$).

Indication that calcium does not participate in the wave of depolarization

Ca^{2+}-dependent mitochondrial depolarizations have been previously described (Duchen et al., 1998; Fall and Bennett, 1999; Leach et al., 2001). We observed that in the rat cardiomyocytes, as the wave of depolarization encompassed the majority of the mitochondrial population, the cell sometimes underwent either a shortening ($n = 2/19$) or hypercontraction ($n = 4/19$), as previously alluded to by Duchen et al. (1998), suggesting that these cells did contain relevant levels of cytosolic calcium. To test for the participation of Ca^{2+} in our model of laser-induced, ROS dependent mitochondrial depolarization, we imaged the wave of depolarization after incubation with the membrane-permeable calcium-chelator, BAPTA-AM (25 μM). BAPTA blocked neither the MPTP-mediated $\Delta\Psi$-fluctuations, nor the wave of depolarization, nor the accompanying increase in ROS production (rat: $n = 3$; rabbit: $n = 5$).

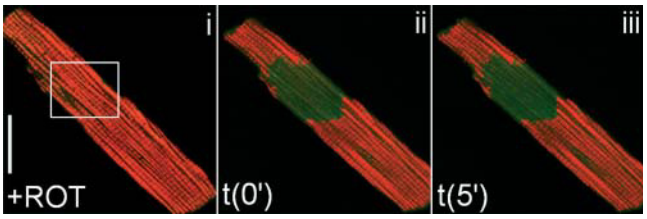

FIGURE 7 Rotenone blocked the wave of depolarization. Rat cardiomyocytes were dual loaded with 10.0 μM $DCFH_2$-DA and 0.1 μM TMRM. Before imaging, cells were incubated for 30 min with 1 μM rotenone. Intense laser photoexcitation resulted in local depolarizations (*B*). (*C*) Subsequently, these depolarizations did not spread during the time period imaged (>5 min). Images were obtained with a Bio-Rad Radiance 2000 LSCM. This is one experiment that is representative of three. Scale bar = 20 μm.

Inhibition of mitochondrial anion channels did not affect the local depolarization but did block the wave

DIDS, an inhibitor of mitochondrial inner membrane anion channels (Beavis and Davatol-Hag, 1996), has been shown to block the release of superoxide anion from the mitochondria into the cytosol (Kulisz et al., 2002). Accordingly, we employed DIDS to test if blocking the release of the MPTP-activated ROS burst from the mitochondrial matrix was sufficient to halt the $\Delta\Psi$-fluctuations and the wave of depolarization in rat cardiomyocyte mitochondria. When submitted to the localized ROS production, DIDS-treated mitochondria still depolarized after TMRM photoexcitation. However, DIDS (100 μM) effectively blocked the spread of depolarization into neighboring mitochondria (our unpublished data; rat: $n = 3$).

DISCUSSION

RIRR, the phenomenon of ROS-activated, MPTP-mediated mitochondrial ROS amplification has been characterized at the level of single cardiomyocyte mitochondria, isolated (Huser et al., 1998) and in situ (Zorov et al., 2000), and in a carcinoma cell line after an initial generation of ROS by irradiation (Leach et al., 2001). However little is known concerning whether the autocatalytic nature of ROS production and the spatial organization of the mitochondria

could ultimately connect the ROS-sensing capability of a few mitochondria to the entire mitochondrial population of a cell.

Our experiments showed that localized RIRR, achieved through TMRM photoexcitation, was indeed communicated to distant mitochondria that had not been subjected to an initial oxidative stress. The localized photoexcitation resulted in either the activation of $\Delta\Psi$-fluctuations (time periods: rat: ~10 min and rabbit ~3 min) or in the more coherent wave of depolarization (velocities: ~5 μm/min). Increased laser power, i.e., enhanced local ROS production, resulted in more waves and fewer cases of the less correlated $\Delta\Psi$-fluctuations. Both $\Delta\Psi$-fluctuations and the wave of mitochondrial depolarization were mediated by the MPTP, as evidenced by calcein permeation and CsA inhibition, and correlated spatially and temporally with increased ROS generation. Apparently ROS participated in the depolarization messenger process: blocking the MPTP, scavenging ROS, or inhibiting the release of ROS from the mitochondrial matrix to the cytosol blocked the spread of mitochondrial depolarization from the region of laser-induced ROS production (see scheme in Fig. 8). Inhibition by rotenone of complex I of the mitochondrial ETC had both the effect of decreasing ROS production and increasing the time to $\Delta\Psi$-collapse during local TMRM photoexcitation (cf. Zorov et al., 2000), as well as blocking the wave of depolarization. This suggests that electrons from the ETC participated in both the localized RIRR described by Zorov et al. and the wave of depolarization described here. Furthermore, the effect of rotenone indicated that progression of the wave of depolarization was due to ETC-dependent changes in $\Delta\Psi$, and thus was not an artifact due to the slow diffusion of bleached TMRM molecules, as might be suggested by those familiar with fluorescence recovery after photobleaching (FRAP).

Close inspection of RIRR at the level of the single mitochondrion, evidenced by both line scanning (our unpublished data) and localized imaging (Fig. 2 *C*), revealed three phases of ROS production. The first phase (*s1*) corresponded to a combination of basal ROS production and ROS generated as a result of photoexcitation. When imaging under conditions that did not activate RIRR, this slope remained constant (our unpublished data). The second phase (*s2*) preceded MPTP activation and continued for the first seconds of MPTP activity in rat (5 ± 2 s) and rabbit (4 ± 2 s) cardiomyocytes. It has previously been shown that bongkrekic acid, which inhibits the MPTP, attenuated this burst in ROS production. This result was taken to suggest that the activation of MPTP caused the ROS burst (Zorov et al., 2000). The third phase (*s3*) was characterized by a decrease in ROS production, and its onset correlated to a collapsed $\Delta\Psi$ (Fig. 2 *C*), which is in agreement with theoretical (Demin et al., 2001) and experimental observations (Aronis et al., 2002). Reinspection of the line scans in Fig. 4, *A* and *B*, published by Zorov et al. (2000) demonstrates a similar triphasic response in terms of ROS production. Although mechanistically the connection between MPTP-activated

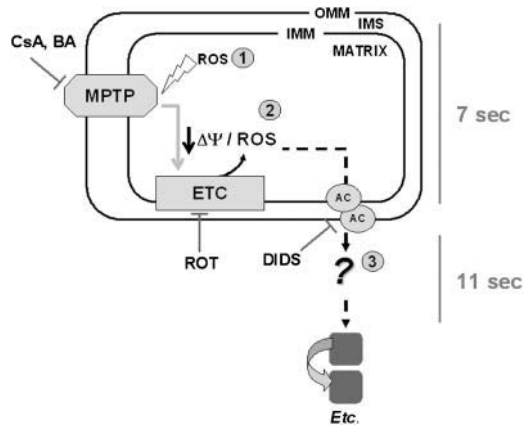

FIGURE 8 Scheme of RIRR and RIRR transmission. At the level of the mitochondrion, RIRR occurred over a period of ~7 s. (*1*) MPTP activation occurs in response to a local increase in ROS. (*2*) MPTP activation results in $\Delta\Psi$-collapse and enhanced ETC ROS generation. (*3*) ROS exits the mitochondrion via AC, located in either the IMM or OMM. A delay of 11 s occurs before activation of RIRR in the neighboring mitochondrion, perhaps evidencing compartmentalized ROS scavenging or a protein mediated RIRR signal relay. Locally RIRR was blocked by CsA, BA, and rotenone (Zorov et al., 2000). Wave transmission was blocked by CsA (Fig. 4 *D*), DIDS (our unpublished data), and ROT (Fig. 7). MPTP, mitochondrial permeability transition pore; ETC, electron transport chain; $\Delta\Psi$, mitochondrial membrane potential; OMM, outer mitochondrial membrane; IMM, inner mitochondrial membrane; IMS, intermembrane space; AC, anion channels; CsA, cyclosporin A; BA, bongkrekic acid; ROT, rotenone.

ROS production is not known, ROS originating from complex III have been shown to be responsible for ANT-mediated MPTP activation (Armstrong and Jones, 2002).

Our observation that DIDS inhibited the spread of mitochondrial depolarization, but not the localized, photoexcitation-induced depolarization, would be consistent with the possibility that $\Delta\Psi$-driven ROS extrusion from the mitochondria, via anion channels in the IMM, communicated RIRR between neighboring mitochondria. As such, simple diffusion of ROS across the IMM should not then suffice for the wave phenomenon to occur. This is in agreement with the finding by Kulisz et al. (2002) that DIDS blocked mitochondria-to-cytosol exit of superoxide anion. Moreover, it is possible that the MPTP was in the active state (open) only during the depolarization phase, which has been measured to take ~4–5 s for a mitochondrion (Table 2). Otherwise ROS could have exited via the MPTP, which permeabilizes the IMM, and DIDS would not have had the observed selective blocking effect on the wave. Indeed, it has been shown that the MPTP is capable of switching from the inactive to the active state and then back to the inactive state in less than 1 s (Zorov et al., 2000; De Giorgi et al., 2002). An alternative explanation is that the MPTP remained open and that ROS could exit the mitochondria, but in the presence of DIDS ROS were not able to enter neighboring mitochondria, activate RIRR, and consequently transmit the wave. This possibility is supported by the finding that DIDS

inhibits the outer membrane voltage dependent anion channel, a component of the MPTP, which appears to at least partially govern superoxide anion progression between the intermembrane space and the cytosol (Han et al., 2003). Although the results obtained using DIDS implicated the superoxide anion in the signaling mechanism, it is not necessarily the active ROS in RIRR. Both $DCFH_2$ (LeBel et al., 1992) and BODIPY $C11^{(581/591)}$ (Pap et al., 1999), which are insensitive to the superoxide anion but sensitive to peroxides, were highly oxidized in our experiments. Furthermore, the scavenging of superoxide anion had no effect on localized RIRR, whereas RIRR was blocked by scavenging H_2O_2 (Zorov et al., 2000).

In most cases, we did not observe any effect of the wave during or immediately after its progression. However, in 4/19 cases wave progression resulted in hypercontraction, likely due to lack of ATP (Koretsune and Marban, 1990). As cytochrome *c* release is known to occur as a result of MPTP activation, it would be of interest to determine whether the RIRR wave in these cases constituted an apoptotic wave of cytochrome *c* release (cf. Pacher and Hajnoczky, 2001). Notably though, in a subset of cells ($n = 8$), we observed that after the wave of mitochondrial depolarization had passed through the entire cell, a sudden cell-wide reemergence (e.g., Fig. 6, 45 $\pm$ 12 μm/min, determined from three cells) of TMRM fluorescence occurred, which we assume to indicate mitochondrial repolarization. This repolarization included the mitochondria that had undergone direct laser-induced depolarization, which suggests that the depolarization wave was compatible with continued mitochondrial function. As the repolarization occurred several minutes after the wave of depolarization, other levels of $\Delta\Psi$-regulation were probably involved. Known possible ROS targets are inactivation of the Krebs cycle (reversible) (Nulton-Persson and Szweda, 2001) and the ETC (Sadek et al., 2002), both of which could reduce $\Delta\Psi$- and ROS production.

When compared to the measured velocities for waves of calcium-induced calcium release, which can range from 10 to 50 μm/s (Rottingen and Iversen, 2000), waves of mitochondrial depolarization, which can traverse a cardiomyocyte at 40 μm/s (calculated from data in Duchen et al., 1998), waves of NAD(P)H oxidation traveling at 2 μm/s (Romashko et al., 1998), or Ca^{2+}-mediated waves of MPTP propagation at $\sim$1 μm/s (Pacher and Hajnoczky, 2001), the wave we report here is strikingly slow at $\sim$0.1 μm/s. Electron microscopy (e.g., Nozaki et al., 2001) and confocal imaging (e.g., Fig. 1) have shown that mitochondria arranged longitudinally along a myofibril are separated by gaps, which we calculated to be 0.4 μm (Table 1). As such, RIRR wave propagation could be considered in terms of both a mitochondrial component (ROS generation) and a cytosolic component (mitochondrion-to-mitochondrion RIRR transmission). We and others (Zorov et al., 2000) observed that RIRR-associated ROS production occurred in mitochondria over a time period of $\sim$7 s, which we assume to be the temporal contribution per mitochondrion. If the wave was strictly mitochondrial, then when examining the longitudinal wave transmission in an confocally determined average cell (length of 118 μm; Table 1), along one myofibril (73 mitochondria), the wave velocity would be $\sim$14 μm/min, $\sim$3 times faster than our reported wave of 5.4 μm/min. Apparently then cytosolic transmission is a factor in wave progression. Based on our determined wave velocity and cardiomyocyte and mitochondrial dimensions (Table 2), the average delay occurring in the cytosolic space between two longitudinally aligned mitochondria, from the end time point of RIRR in one mitochondrion to the start of RIRR in the neighboring mitochondrion, would then be $\sim$11 s (see calculations in Table 2).

ROS-sensitive fluorescent dyes (Figs. 5 and 6), scavengers (our unpublished data), and rotenone (Fig. 7) identified ROS as a component in the transmission of RIRR. Although H_2O_2, with a diffusion coefficient of 1.3 μm^2/s (Henzler and Steudle, 2000), could cross the gap of 0.4 μm within the required time, both its highly reactive nature and the slowness of the wave argue against it serving as a simple diffusible second messenger. It is possible that ROS scavenging by the cytosolic antioxidant system might take some time to become locally saturated, and only after this saturation could the excess ROS be able to diffuse and activate the neighboring mitochondria. A related possibility is that basal ROS generation in neighboring mitochondria (Boveris et al., 1972) increased due to local saturation, reaching a level sufficient to self-trigger the MPTP, as shown to occur when glutathione (GSH) is experimentally depleted (Armstrong and Jones, 2002).

Although we discuss average wave velocities, there were clear examples of heterogeneity in wave progression. Wave velocity apparently was greatest after wave activation, and slowing thereafter, as demonstrated by the curvature of the line in Fig. 5 *B*. However, the identity of the factors that contributed to the slowing of the wave, such as the gradual cell-wide depletion of NADH (thus source of electrons for ROS production), enhanced ROS scavenging, or decreased MPTP activity remain to be elucidated.

Furthermore, wave progression was at times saltatory. Mitochondria that were distal to the wave front occasionally depolarized (*closed arrows* in Fig. 5 *B*) or remained polarized behind the wave front (*open arrows* in Fig. 5 *B*) and several mitochondria within the same row depolarized in a coordinated manner (*dashed arrow* in Fig. 5 *B*). When examining the pattern of depolarization between a degree of coordination among mitochondria was observed at the subsecond timescale (see Supplementary Video 1), as previously reported (Zorov et al., 2000). These patterns are indicative of mitochondria interconnectivity above and/or below the confocal plane we imaged. Although intermitochondrial coupling has been postulated (Skulachev, 2001), we consider this unlikely. Localized depolarization within a mitochondrial reticulum leads to a virtually instantaneous depolarization of coupled mitochondria (e.g., Amchenkova

et al., 1988). Thus, given the slow wave velocity we report here, $\Delta\Psi$-sharing among the majority of mitochondria was not occurring. However, we consistently observed that, after localized RIRR, neighboring mitochondria initially remained polarized, in both the longitudinal and lateral directions (e.g., Figs. 4 *C* and 5 *A*). The apparent lack of mitochondrial connectivity is also supported by the persistent bleached line in Fig. 4 *C*. This result suggested that calcein was to an important extent immobilized within both the mitochondria and the cytosol. If mitochondrial connectivity were occurring, the diffusion of mitochondrial calcein should have resulted in a recovery of fluorescence in the targeted region. We thus propose that apparent coordinated depolarizations do not evidence rows of electrically united mitochondria but originate from the heterogeneous RIRR response to oxidative stress (e.g., depolarization pattern in Supplementary Video 1). Depolarizations occurring distal to the wave front likely occur due to RIRR transmission above or below the imaged confocal plane. However, experiments employing techniques to probe mitochondria matrix continuity using fluorescence recovery after photobleaching should be undertaken to clarify this issue (Collins and Bootman, 2003).

Although in certain cell types Ca^{2+} participation appears essential to activate waves of mitochondrial depolarization (Ichas et al., 1997; Duchen et al., 1998; Leach et al., 2001; Pacher and Hajnoczky, 2001), apparently Ca^{2+} was not necessary in our experiments: ROS-activated, MPTP-mediated mitochondrial depolarizations occurred after the incubation with BAPTA-AM. This result is somewhat surprising as Ca^{2+} is classically considered to be the most important factor in MPTP activation, with oxidative stress functioning to sensitize the MPTP to Ca^{2+} (see review by Crompton, 1999). However, oxidative stress has been shown to induce the MPT also in the absence of Ca^{2+} (Huser et al., 1998; Zorov et al., 2000), and glutathione depletion alone is sufficient to induce its activation (Armstrong and Jones, 2002). These results suggest that the MPT occurs as a graded response to oxidative stress. Such a concept is highlighted by a decrease of CsA sensitivity in experiments using TMRM photoexcitation to trigger the MPTP. In isolated mitochondria, the CsA inhibitory effect is lessened over time (Huser et al., 1998), and we observed that CsA did not affect the depolarizing mitochondria in the region of laser-induced oxidative stress but blocked the resulting wave of depolarization from spreading (Fig. 4). Thus, at least in the rat and rabbit cardiomyocyte, ROS may be a sufficient, depolarizing messenger, in response to a large enough, localized ROS production.

Recently it was reported that localized ROS production within mitochondria activated prolonged $\Delta\Psi$-oscillations of surrounding mitochondria (Aon et al., 2003). However, the oscillations and wave appear to be controlled differently by relevant factors. In the conditions that gave rise to the wave (our study) antimycin A, an ETC complex III inhibitor, blocked the laser-induced depolarization and ROS production (our unpublished data), whereas Aon et al. reported that antimycin A potentiated their oscillations. Cyclosporin A, which blocked the wave in our study, did not affect the oscillations and calcein permeability in the study by Aon et al. In regards to the time correlation of mitochondrial depolarization, in our study approximately three mitochondria depolarized per minute, whereas the depolarization of the majority of mitochondria in the study of Aon et al. occurred on the second timescale. Also, in a number of cases in our study the phenomenon was reversible in the sense that all mitochondria in the cell returned to a polarized state, after some 10 min (in the study by Aon et al., the laser challenged mitochondria remained depolarized). Perhaps activation of MPTP-mediated wave versus MPTP-independent $\Delta\Psi$-oscillations depends on a higher level of ROS generation. Indeed, we found that higher initial ROS generation favored CsA-sensitive waves over oscillations.

CONCLUSIONS

Cardiomyocyte mitochondria are well known to respond to both hypoxia (Vanden Hoek et al., 1997) and the ischemia-reperfusion transition (Zweier et al., 1987) with increased ROS production. Similar to the propagation of mitochondrial depolarization and ROS production reported here for the isolated cardiomyocyte and by Aon et al. (2003), rotenone (Becker et al., 1999), and DIDS (Vanden Hoek et al., 1998) also inhibit ROS production in models of ischemia and preconditioning, respectively. Together these results reveal a complex system of intracellular mitochondrial communication, and clearly demonstrate that mitochondrial ROS production can be a propagated event through an entire cell and even to an adjacent connected cardiomyocyte, likely through the gap junctional complex (our unpublished data). We speculate that communicability of RIRR may be part of the capability of the cell to sense and assess the degree of ROS damage, both spatially and temporally. Future experiments will be aimed at determining whether the different degrees of RIRR (MPTP-independent versus MPTP-mediated; oscillations versus wave) might indicate the different levels of coordination amongst mitochondria needed to communicate (pre)apoptotic (cf. Pacher and Hajnoczky, 2001) or preconditioning signals throughout the cell.

SUPPLEMENTARY MATERIAL

An online supplement to this article can be found by visiting BJ Online at http://www.biophysj.org.

We are grateful to H. Dekker, J. Lankelma, C. Woldringh, and P. van der Smissen for help with confocal microscopy, C. Beauloye, D. Meisse, A. Ginion, and L. Maisin for help with the rat cardiomyocyte preparation, and G. Wardeh for a supply of rat hearts. We also thank M. van Borren and others at the Amsterdam Medical Centrum for the gift of the isolated rabbit cardiomyocytes.

This work was supported by a Breedtestrategie grant from the Free University Amsterdam, by the Netherlands Organisation for Scientific Research (Foundation for Physics Research/Research Council for Earth and Life Science/Physical Biology), by the Belgian Federal Program of Interuniversity Poles of Attraction (P5), by the Belgian Fund for Medical Scientific Research, and by the ''Actions de Recherche Concertees'' 98/03-216 (French Community of Belgium).

REFERENCES

Amchenkova, A. A., L. E. Bakeeva, Y. S. Chentsov, V. P. Skulachev, and D. B. Zorov. 1988. Coupling membranes as energy-transmitting cables. I. Filamentous mitochondria in fibroblasts and mitochondrial clusters in cardiomyocytes. *J. Cell Biol.* 107:481–495.

Aon, M. A., S. Cortassa, E. Maraban, and B. O'Rourke. 2003. Synchronized whole-cell oscillations in mitochondrial metabolism triggered by a local release of reactive oxygen species in cardiac myocytes. *J. Biol. Chem.* 278:44735–44744.

Armstrong, J. S., and D. P. Jones. 2002. Glutathione depletion enforces the mitochondrial permeability transition and causes cell death in Bcl-2 overexpressing HL60 cells. *FASEB J.* 16:1263–1265.

Aronis, A., R. Komarnitsky, S. Shilo, and O. Tirosh. 2002. Membrane depolarization of isolated rat liver mitochondria attenuates permeability transition pore opening and oxidant production. *Antioxid. Redox. Signal.* 4:647–654.

Beavis, A. D., and H. Davatol-Hag. 1996. The mitochondrial inner membrane anion channel is inhibited by DIDS. *J. Bioenerg. Biomembr.* 28:207–214.

Becker, L. B., T. L. vanden Hoek, Z. H. Shao, C. Q. Li, and P. T. Schumacker. 1999. Generation of superoxide in cardiomyocytes during ischemia before reperfusion. *Am. J. Physiol.* 277(Pt. 2):H2240–H2246.

Boitier, E., R. Rea, and M. R. Duchen. 1999. Mitochondria exert a negative feedback on the propagation of intracellular Ca2+ waves in rat cortical astrocytes. *J. Cell Biol.* 145:795–808.

Boveris, A., N. Oshino, and B. Chance. 1972. The cellular production of hydrogen peroxide. *Biochem. J.* 128:617–630.

Collins, T. J., and M. D. Bootman. 2003. Mitochondria are morphologically heterogeneous within cells. *J. Exp. Biol.* 206:1993–2000.

Crompton, M. 1999. The mitochondrial permeability transition pore and its role in cell death. *Biochem. J.* 341:233–249.

De Giorgi, F., L. Lartigue, M. K. Bauer, A. Schubert, S. Grimm, G. T. Hanson, S. J. Remington, R. J. Youle, and F. Ichas. 2002. The permeability transition pore signals apoptosis by directing Bax translocation and multimerization. *FASEB J.* 16:607–609.

Demin, O. V., I. I. Gorianin, B. N. Kholodenko, and H. V. Westerhoff. 2001. Kinetic modeling of energy metabolism and generation of active forms of oxygen in hepatocyte mitochondria. *Mol Biol (Mosk).* 35:1095–1104.

Duchen, M. R., A. Leyssens, and M. Crompton. 1998. Transient mitochondrial depolarizations reflect focal sarcoplasmic reticular calcium release in single rat cardiomyocytes. *J. Cell Biol.* 142:975–988.

Elmore, S. P., T. Qian, S. F. Grissom, and J. J. Lemasters. 2001. The mitochondrial permeability transition initiates autophagy in rat hepatocytes. *FASEB J.* 15:2286–2287.

Fall, C. P., and J. P. Bennett. 1999. Visualization of cyclosporin A and Ca2+-sensitive cyclical mitochondrial depolarizations in cell culture. *Biochim. Biophys. Acta.* 1410:77–84.

Han, D., F. Antunes, R. Canali, D. Rettori, and E. Cadenas. 2003. Voltage-dependent anion channels control the release of the superoxide anion from mitochondria to cytosol. *J. Biol. Chem.* 278:5557–5563.

Henzler, T., and E. Steudle. 2000. Transport and metabolic degradation of hydrogen peroxide in Chara corallina: model calculations and measurements with the pressure probe suggest transport of H2O2 across water channels. *J. Exp. Bot.* 51:2053–2066.

Huser, J., and L. A. Blatter. 1999. Fluctuations in mitochondrial membrane potential caused by repetitive gating of the permeability transition pore. *Biochem. J.* 343:311–317.

Huser, J., C. E. Rechenmacher, and L. A. Blatter. 1998. Imaging the permeability pore transition in single mitochondria. *Biophys. J.* 74:2129–2137.

Ichas, F., L. S. Jouaville, and J. P. Mazat. 1997. Mitochondria are excitable organelles capable of generating and conveying electrical and calcium signals. *Cell.* 89:1145–1153.

Koretsune, Y., and E. Marban. 1990. Mechanism of ischemic contracture in ferret hearts: relative roles of [Ca2+]i elevation and ATP depletion. *Am. J. Physiol.* 258:H9–16.

Kulisz, A., N. Chen, N. S. Chandel, Z. Shao, and P. T. Schumacker. 2002. Mitochondrial ROS initiate phosphorylation of p38 MAP kinase during hypoxia in cardiomyocytes. *Am. J. Physiol. Lung Cell. Mol. Physiol.* 282:L1324–L1329.

Leach, J. K., G. Van Tuyle, P. S. Lin, R. Schmidt-Ullrich, and R. B. Mikkelsen. 2001. Ionizing radiation-induced, mitochondria-dependent generation of reactive oxygen/nitrogen. *Cancer Res.* 61:3894–3901.

LeBel, C. P., H. Ischiropoulos, and S. C. Bondy. 1992. Evaluation of the probe 2′,7′-dichlorofluorescin as an indicator of reactive oxygen species formation and oxidative stress. *Chem. Res. Toxicol.* 5:227–231.

Lefebvre, V., M. C. Mechin, M. P. Louckx, M. H. Rider, and L. Hue. 1996. Signaling pathway involved in the activation of heart 6-phosphofructo-2-kinase by insulin. *J. Biol. Chem.* 271:22289–22292.

Lemasters, J. J., A. L. Nieminen, T. Qian, L. C. Trost, S. P. Elmore, Y. Nishimura, R. A. Crowe, W. E. Cascio, C. A. Bradham, D. A. Brenner, and B. Herman. 1998. The mitochondrial permeability transition in cell death: a common mechanism in necrosis, apoptosis and autophagy. *Biochim. Biophys. Acta.* 1366:177–196.

Nieminen, A. L., A. K. Saylor, S. A. Tesfai, B. Herman, and J. J. Lemasters. 1995. Contribution of the mitochondrial permeability transition to lethal injury after exposure of hepatocytes to t-butylhydroperoxide. *Biochem. J.* 307:99–106.

Nozaki, T., Y. Kagaya, N. Ishide, S. Kitada, M. Miura, J. Nawata, I. Ohno, J. Watanabe, and K. Shirato. 2001. Interaction between sarcomere and mitochondrial length in normoxic and hypoxic rat ventricular papillary muscles. *Cardiovasc. Pathol.* 10:125–132.

Nulton-Persson, A. C., and L. I. Szweda. 2001. Modulation of mitochondrial function by hydrogen peroxide. *J. Biol. Chem.* 276:23357–23361.

Pacher, P., and G. Hajnoczky. 2001. Propagation of the apoptotic signal by mitochondrial waves. *EMBO J.* 20:4107–4121.

Pap, E. H., G. P. Drummen, V. J. Winter, T. W. Kooij, P. Rijken, K. W. Wirtz, J. A. Op den Kamp, W. J. Hage, and J. A. Post. 1999. Ratio-fluorescence microscopy of lipid oxidation in living cells using C11-BODIPY(581/591). *FEBS Lett.* 453:278–282.

Romashko, D. N., E. Marban, and B. O'Rourke. 1998. Subcellular metabolic transients and mitochondrial redox waves in heart cells. *Proc. Natl. Acad. Sci. USA.* 95:1618–1623.

Rottingen, J.-A., and J.-G. Iversen. 2000. Ruled by waves? Intracellular and intercellular calcium signalling. *Acta Physiol. Scand.* 169:203–219.

Sadek, H., K. Humphries, P. Szweda, and L. Szweda. 2002. Selective inactivation of redox-sensitive mitochondrial enzymes during cardiac reperfusion. *Arch. Biochem. Biophys.* 406:222–228.

Skulachev, V. P. 2001. Mitochondrial filaments and clusters as intracellular power-transmitting cables. *Trends Biochem. Sci.* 26:23–29.

Sutovsky, P., C. S. Navara, and G. Schatten. 1996. Fate of the sperm mitochondria, and the incorporation, conversion, and disassembly of the sperm tail structures during bovine fertilization. *Biol. Reprod.* 55:1195–1205.

Swift, L. M., and N. Sarvazyan. 2000. Localization of dichlorofluorescin in cardiac myocytes: implications for assessment of oxidative stress. *Am. J. Physiol.* 278:H982–H990.

Vanden Hoek, T. L., L. B. Becker, Z. Shao, C. Li, and P. T. Schumacker. 1998. Reactive oxygen species released from mitochondria during brief

hypoxia induce preconditioning in cardiomyocytes. *J. Biol. Chem.* 273:18092–18098.

Vanden Hoek, T. L., C. Li, Z. Shao, P. T. Schumacker, and L. B. Becker. 1997. Significant levels of oxidants are generated by isolated cardiomyocytes during ischemia prior to reperfusion. *J. Mol. Cell. Cardiol.* 29:2571–2583.

Verheijck, E. E., A. C. G. van Ginneken, R. Wilders, and L. N. Bouman. 1999. Contribution of L-type Ca2+ current to electrical activity in sinoatrial nodal myocytes of rabbits. *Am. J. Physiol.* 276:H1064–H1077.

Zoratti, M., and I. Szabo. 1995. The mitochondrial permeability transition. *Biochim. Biophys. Acta.* 1241:139–176.

Zorov, D. B., C. R. Filburn, L. O. Klotz, J. L. Zweier, and S. J. Sollott. 2000. Reactive oxygen species (ROS)-induced ROS release: a new phenomenon accompanying induction of the mitochondrial permeability transition in cardiac myocytes. *J. Exp. Med.* 192:1001–1014.

Zweier, J. L., J. T. Flaherty, and M. L. Weisfeldt. 1987. Direct measurement of free radical generation following reperfusion of ischemic myocardium. *Proc. Natl. Acad. Sci. USA.* 84:1404–1407.